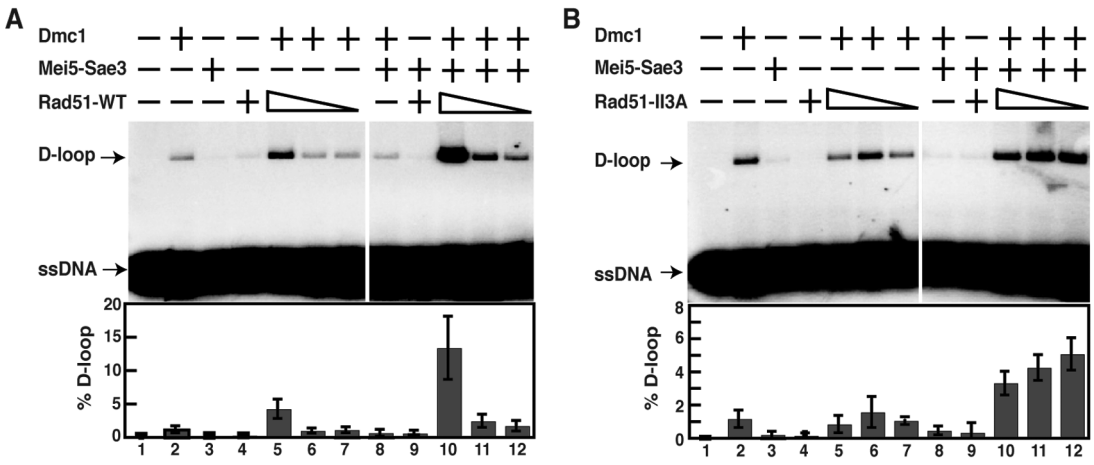

Fig. 4. Rad51 stimulates Dmc1's D-loop activity. Dmc1 (1 μM) was preincubated with or without Rad51-WT (**A**) or Rad51-II3A (**B**) (0.5, 0.1, and 0.02 μM), Mei5-Sae3 (0.5 μM), and ^{32}P-labeled 90-mer ssDNA (3.6 μM nucleotides). Plasmid pRS306 (22 μM base pairs) was then added to initiate D-loop formation. Error bars represent SEM, $N = 4$.

partnerships between meiosis-specific proteins and their mitotically active paralogs.

References and Notes

1. D. K. Bishop, D. Park, L. Xu, N. Kleckner, *Cell* **69**, 439 (1992).
2. A. Shinohara, H. Ogawa, T. Ogawa, *Cell* **69**, 457 (1992).
3. A. Schwacha, N. Kleckner, *Cell* **90**, 1123 (1997).
4. S. Sheridan, D. K. Bishop, *Genes Dev.* **20**, 1685 (2006).
5. H. Tsubouchi, G. S. Roeder, *Genes Dev.* **20**, 1766 (2006).
6. B. Müller, T. Koller, A. Stasiak, *J. Mol. Biol.* **212**, 97 (1990).
7. H. Kurumizaka, S. Ikawa, A. Sarai, T. Shibata, *Arch. Biochem. Biophys.* **365**, 83 (1999).
8. P. Chi, S. Van Komen, M. G. Sehorn, S. Sigurdsson, P. Sung, *DNA Repair (Amsterdam)* **5**, 381 (2006).
9. J. San Filippo, P. Sung, H. Klein, *Annu. Rev. Biochem.* **77**, 229 (2008).
10. S. L. Gasior, A. K. Wong, Y. Kora, A. Shinohara, D. K. Bishop, *Genes Dev.* **12**, 2208 (1998).
11. D. K. Bishop, *Cell* **79**, 1081 (1994).
12. A. Shinohara, S. Gasior, T. Ogawa, N. Kleckner, D. K. Bishop, *Genes Cells* **2**, 615 (1997).
13. S. D. Oh *et al.*, *Cell* **130**, 259 (2007).
14. S. R. Ferrari, J. Grubb, D. K. Bishop, *J. Biol. Chem.* **284**, 11766 (2009).
15. A. Hayase *et al.*, *Cell* **119**, 927 (2004).
16. A. F. Say *et al.*, *DNA Repair (Amsterdam)* **10**, 586 (2011).
17. Y. Kokabu *et al.*, *J. Biol. Chem.* **286**, 43569 (2011).
18. N. Hunter, N. Kleckner, *Cell* **106**, 59 (2001).

Acknowledgments: We are grateful to A. Zhang and P. Rice for structural alignments, N. Hunter for critical reading of the manuscript and strains, P. Sung for plasmid pET11d-ScRad52, and W. Heyer for Rad54 protein. This work was supported by National Institute for General Medical Sciences grant GM50936.

Supplementary Materials

www.sciencemag.org/cgi/content/full/337/6099/1222/DC1
Materials and Methods
Figs. S1 to S8
Tables S1 and S2
References (*19*–*26*)

19 January 2012; accepted 5 July 2012
10.1126/science.1219379

The Molecular Mechanism of Thermal Noise in Rod Photoreceptors

Samer Gozem,[1] Igor Schapiro,[1] Nicolas Ferré,[2] Massimo Olivucci[1,3]*

Spontaneous electrical signals in the retina's photoreceptors impose a limit on visual sensitivity. Their origin is attributed to a thermal, rather than photochemical, activation of the transduction cascade. Although the mechanism of such a process is under debate, the observation of a relationship between the maximum absorption wavelength (λ_{max}) and the thermal activation kinetic constant (k) of different visual pigments (the Barlow correlation) indicates that the thermal and photochemical activations are related. Here we show that a quantum chemical model of the bovine rod pigment provides a molecular-level understanding of the Barlow correlation. The transition state mediating thermal activation has the same electronic structure as the photoreceptor excited state, thus creating a direct link between λ_{max} and k. Such a link appears to be the manifestation of intrinsic chromophore features associated with the existence of a conical intersection between its ground and excited states.

Rhodopsin (Rh), a heterotrimeric G protein—coupled receptor found in rod cells of the eye, is responsible for vision in dim light. It comprises an opsin apoprotein and the 11-cis retinal protonated Schiff base (PSB11) chromophore covalently linked to the opsin core. Visual pigments of the Rh family mediate vision in all seeing animals (*1*). The activation of visual pigments is normally triggered by the photochemical isomerization of PSB11 to the corresponding all-trans isomer (PSBAT) within the opsin retinal binding pocket (*2*), yielding the ground state (S_0) photocycle intermediate bathoRh. Spectroscopic studies have established that in the prototypical pigment bovine Rh, the isomerization occurs on a femtosecond time scale (*3*–*5*). The additional observation of S_0 vibrational coherence (*6*) supports a direct transfer of the excited-state (S_1) population to the photoproduct along a downhill path passing through a conical intersection (CI). Such a path has been located along the Rh potential energy surfaces, using multiconfigurational quantum chemical (MCQC) calculations (*7*–*9*), and has been spectroscopically supported by probing in the infrared (*9*). As outlined in Fig. 1, the resulting photochemical isomerization mechanism is qualitatively different from that of a thermal isomerization, which is expected to be controlled by an energy barrier (E_a^T, thermal activation energy) corresponding to an S_0 transition state (TS) with diradical character (*10*).

In contrast to light activation, the mechanism of thermal activation of visual pigments has not been established. One reason for the ongoing debate is the discrepancy between the measured activation barrier in toad Rh (~22 kcal/mol) (*11*) and the observed energy storage in bovine bathoRh (~32 kcal/mol) (*12*). Because E_a^T for PSB11 in opsin cannot be lower than the product energy, it has been suggested that the thermal mechanism bypasses bathoRh production (*13*). However, there is compelling evidence that the thermal and photochemical activations are mechanistically related. First, the signal triggered by thermal activation is indistinguishable from that caused by light (*11*). Second, as for light activation, the thermal process leads to PSB11 isomerization without substantially changing the secondary structure of the opsin (*14*). The observations above question the validity of the measured activation barrier. Ala-Laurila *et al.* (*15*) and, more recently,

[1]Department of Chemistry, Bowling Green State University, Bowling Green, OH 43403, USA. [2]Institut de Chimie Radicalaire, UMR 7273–Université d'Aix-Marseille, 13397 Marseille Cedex 20, France. [3]Dipartimento di Chimica, Università di Siena, via De Gasperi 2, I-53100 Siena, Italy.

*To whom correspondence should be addressed. E-mail: molivuc@bgsu.edu, olivucci@unisi.it

Luo *et al.* (*16*) have suggested that the barrier value (*11*) is incorrect because it assumes Boltzmann statistics. On the other hand, a computational study by Khrenova *et al.* (*10*) suggests that the barrier is correct but the stored energy is not.

A number of studies have tried to resolve the above discrepancies by proposing more complex mechanisms for the thermal activation, such as an isomerization occurring in an Rh population where the chromophore is deprotonated (*17*), simultaneous hydrolysis and thermal isomerization of PSB11 (*14*), a change in the hydrogen-bonding network near the active site (*18*), fluctuations in the protein structure (*19*), or bioluminescence near the retina (*20*). More recent computations indicate that the S_1 state may be thermally accessed (*21*). However, these mechanistic models do not explicitly address the experimentally observed Barlow correlation (*22*, *23*), which establishes a relationship between the pigment thermal activation kinetic constant (k) and the maximum absorption wavelength (λ_{max}), such that $-\log k$ is directly proportional to $1/\lambda_{max}$. This provides a link between thermal and photochemical activation (*15*, *16*) that any correct mechanism must explain.

The importance of accounting for the Barlow correlation is emphasized by Luo *et al.* (*16*), who have provided quantitative evidence of its validity. Adopting a theory presented by Ala-Laurila *et al.* (*15*), they proposed that the observed thermal activation measurements could be described using a $\log k = \log A(E_a^T, T) - E_a^T/RT$ law (A, pre-exponential factor; T, absolute temperature; R, gas constant) and assumed that $E_a^T = E_a^P$, where E_a^P is an experimentally established function of $1/\lambda_{max}$ called the photochemical energy barrier (*23*). Because the authors associate E_a^P with the minimal photon energy capable of triggering the isomerization, the $E_a^T = E_a^P$ assumption could be interpreted to mean that energy from photons is used to follow the thermal isomerization path. However, this contradicts the established CI-driven S_1 isomerization of Fig. 1, which avoids E_a^T. Furthermore, E_a^P must be a quantity close to the 0-0 excitation energy (i.e., the energy gap between the S_0 and S_1 minima) and far from the S_0 energy barrier (fig. S1). Clearly, the observed proportionality between $-\log k$ and $1/\lambda_{max}$ must reflect a different mechanism. Assuming, consistently with Luo *et al.* (*16*), that chromophore isomerization drives the thermal activation, such a mechanism must explain the relationship between E_a^T and $1/\lambda_{max}$ on the basis of the geometrical and electronic properties of opsin-embedded PSB11.

MCQC calculations allow the computation of E_a^T and $1/\lambda_{max}$ from first principles by locating the pigment equilibrium and TS structures. Computation of these quantities for a set of 12 pigments explains the link between E_a^T and $1/\lambda_{max}$ in terms of the charge distribution of their chromophores. MCQC-based quantum mechanics/molecular mechanics (QM/MM) calculations on bovine Rh show that S_0 PSB11 has a +0.86 e charge residing on the Schiff base moiety (Fig. 1). Vertical excitation to S_1 transfers about 30% of this charge toward the β-ionone moiety. This difference in charge distribution explains the sensitivity of λ_{max} [and corresponding vertical excitation energy $\Delta E(S_1 - S_0)$] to the opsin sequence. Sequences that stabilize the positive charge in the Schiff base region would blueshift the absorption, whereas sequences that stabilize the charge on the β-ionone region would redshift the absorption. Because $-\log k$ is seen to increase linearly as a function of $1/\lambda_{max}$ (*16*), the correct thermal activation mechanism should explain why opsins decreasing E_a^T would also decrease $\Delta E(S_1 - S_0)$, and increasing E_a^T would also increase $\Delta E(S_1 - S_0)$.

As previously reported (*24*), the S_0 potential energy surface of a gas-phase PSB11 model features two TSs [TS_{DIR} and TS_{CT} (DIR, diradical; CT, charge transfer)] controlling the same thermal isomerization (Fig. 2A). In Fig. 2B, we present the TS_{DIR} and TS_{CT} structures computed for bovine Rh using a MCQC/AMBER QM/MM model, in which all the side chains and waters of the chromophore binding pocket are relaxed (figs. S2 to S9) (*25*). The necessarily approximated MCQC levels used to compute the TS geometry (CASSCF/6-31G*) and barriers (CASPT2//CASSCF/6-31G*) have been validated by mapping the S_0 energy surface of a reduced PSB11 model up to the CASPT2/6-31G* and MRCISD+Q/6-31++G** levels, respectively (fig. S8). TS_{DIR} features the structure expected for a homolytically broken double bond with two radical centers delocalized along orthogonal π-systems and corresponds to the TS of Fig. 1. As expected, its charge distribution correlates with that of the S_0 PSB11 reactant, with a +0.98 e charge localized in the Schiff base region. In contrast, TS_{CT} has most of its charge (+0.90 e) located on the β-ionone region and thus more closely resembles the charge distribution of vertically excited S_1 PSB11 (compare the corresponding bubble diagrams in Figs. 2A and 1). We find that TS_{CT} has a computed activation energy of 34 kcal/mol and, unexpectedly, lies 11 kcal/mol in energy below TS_{DIR} (fig. S9). Although this value depends on the MCQC level used in the calculation, an increase in the level of theory invariably leads to a larger stabilization of TS_{CT} (figs. S7 to S9) Therefore, TS_{CT} has full control of the thermal isomerization.

The close electronic characters of TS_{CT} and of the opsin-embedded S_1 PSB11 (i.e., a positive charge preferentially localized on the β-ionone region) provide a direct link between E_a^T and $\Delta E(S_1 - S_0)$ and, in turn, $-\log k$ and $1/\lambda_{max}$. The link is derived from first-principles quantum-mechanical computations and makes the $E_a^T = E_a^P$ assumption (*16*) [and even its more permissive $E_a^T = \alpha E_a^P - \beta$ form, where α and β are constants (*15*, *16*)] unnecessary. Accordingly, any opsin redshifting the absorption would simultaneously decrease E_a^T. The opposite behavior, not consistent with the Barlow correlation, would be observed if the isomerization were controlled by TS_{DIR}. In order to support these conjectures, we display in Fig. 2C the E_a^T versus $1/\lambda_{max}$ correlation computed by modeling a set of pigments. These are five bovine Rh (A1-Rh) mutants and six derivatives featuring the 3,4-dehydro-retinal (A2) chromophore. The QM/MM-derived correlation supports the conclusion that TS_{CT} and S_1 PSB11 have similar charge distributions, displaying a clear positive slope exclusively for the TS_{CT} barriers and closely reproducing the slope of the experimentally derived $E_a^T = 0.84\ hc/\lambda_{max}$ relation (h, Planck's constant; c, speed of light) (*16*) (dashed line in Fig. 2C). The E_a^T values

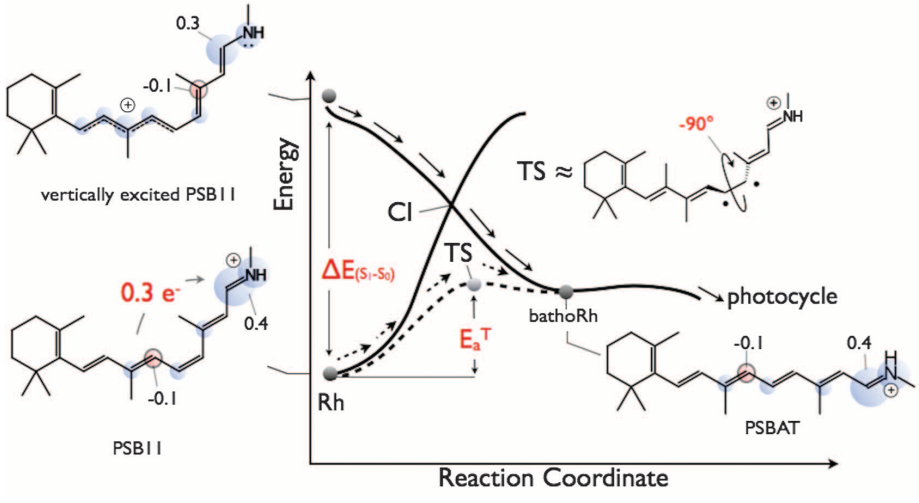

Fig. 1. Schematic representation of the photochemical (solid arrows) and thermal (dashed arrows) isomerization paths. The CI is located energetically above the TS (assumed to have a diradical character), features a different geometrical structure, and drives a far-from-equilibrium process. The CASSCF/6-31G*/AMBER S_0 and S_1 Mulliken charge distributions along the backbone of the bovine Rh chromophore (PSB11) are represented with bubble diagrams on the left of the graph. The labels indicate the maximum and minimum values for the charges. The bond-line formulas represent the dominant electronic configurations of the corresponding states (wavefunctions).

associated with TS_{CT} are therefore proportional to the values derived under the $E_a^T = E_a^P$ assumption.

Although the positive slope characterizing the Barlow correlation is controlled by the changes in E_a^T, the quantitative simulation of the $-\log k$ versus $1/\lambda_{max}$ relationship from first principles requires the computation of the pre-exponential $A(E_a^T, T)$. Although this can be attempted by using TS theory, such a calculation is impractical for molecules the size of visual pigments. Using the computed E_a^T values and assuming the validity of the same Hinshelwood kinetic model originally proposed by Ala-Laurila *et al.* (*15*) and adopted in Luo *et al.* (*16*) to account for the effect of the chromophore vibrational modes, we calculated five A1/A2-Rh rate-constant ratios: 1/8.3 [wild type (WT)], 1/7.3 [$Ala^{269} \rightarrow Thr^{269}$ (A269T)], 1/9.3 (F261Y), 1/9.7 (E113D), and 1/301.2 (T118A) to be compared to the measured ratio between A1 *Bufo* Rh and A2 *Xenopus* Rh of 1/8.9. Using the same Hinshelwood model, a quantitative fit to the observed k versus λ_{max} data for visual pigments was achieved (fig. S10). The computed barriers and rate-constant ratios were obtained via QM/MM models of the pigments and do not contain experimental parameters. The large deviation of T118A from the observed ratio is tentatively assigned to an overestimated barrier for the A1 chromophore.

Thus, the Barlow correlation is explained naturally by considering the quantum-mechanical properties of PSB11. Because the Barlow correlation appears to be generally valid for visual pigments, we conclude that in these systems, TS_{CT}, rather than TS_{DIR}, controls the thermal isomerization. However, the data of Fig. 2C predict that TS_{DIR} will control thermal isomerization for λ_{max} below 470 nm (after accounting for a systematic ~3.2 kcal/mol blueshift in our computed excitation energy), yielding an anti-Barlow correlation, seen as a negative slope in the diagram of Fig. 2C. The same results provide evidence that the rate-determining step controlling the thermal noise must be the canonical PSB11 isomerization, in agreement with the Luo *et al.* (*16*) hypothesis. As discussed in Luo *et al.* (*16*), the observed correlation is not necessarily incompatible with the previously reported 22 kcal/mol apparent activation energy because, in that case, an energy- and temperature-independent pre-exponential factor was assumed (*11*). Also, the computed 34 kcal/mol barrier for TS_{CT} has uncertainty of a few kilocalories per mole because of the MCQC computational error (fig. S8) and the fact that we have used a rather stiff protein model (only the cavity residues are relaxed during the calculations). Our conclusions are also not incompatible with a recently proposed noise model based on protein fluctuations (*19*) or models in which the magnitude of the noise is sensitive to the opsin hydrogen bond network (*18*) (fig. S11), provided that PSB11 isomerization remains the kinetic bottleneck. Finally, the hypothesis that the Barlow correlation is a chromophore property is supported by similar relationships observed for the 13-cis chromophore in solution and in bacterioRh (*26*).

In 1963, Herzberg and Longuet-Higgins showed that the electronic wavefunctions of two states crossing at a CI undergo large changes when moving the molecular structure along a loop encircling a single CI point (*27*). As pictorially illustrated in Fig. 2A, one consequence of their geometric-phase theorem is that such wavefunctions exchange character (*28*) when the molecular structure is displaced from one side to the opposite side of the CI lower cone. This behavior has been computationally demonstrated for PSB11 (*29*) where, near the intersection, S_0 has a covalent/diradical character (ψ_{DIR}), whereas S_1 has a charge-transfer character (ψ_{CT}). Thus,

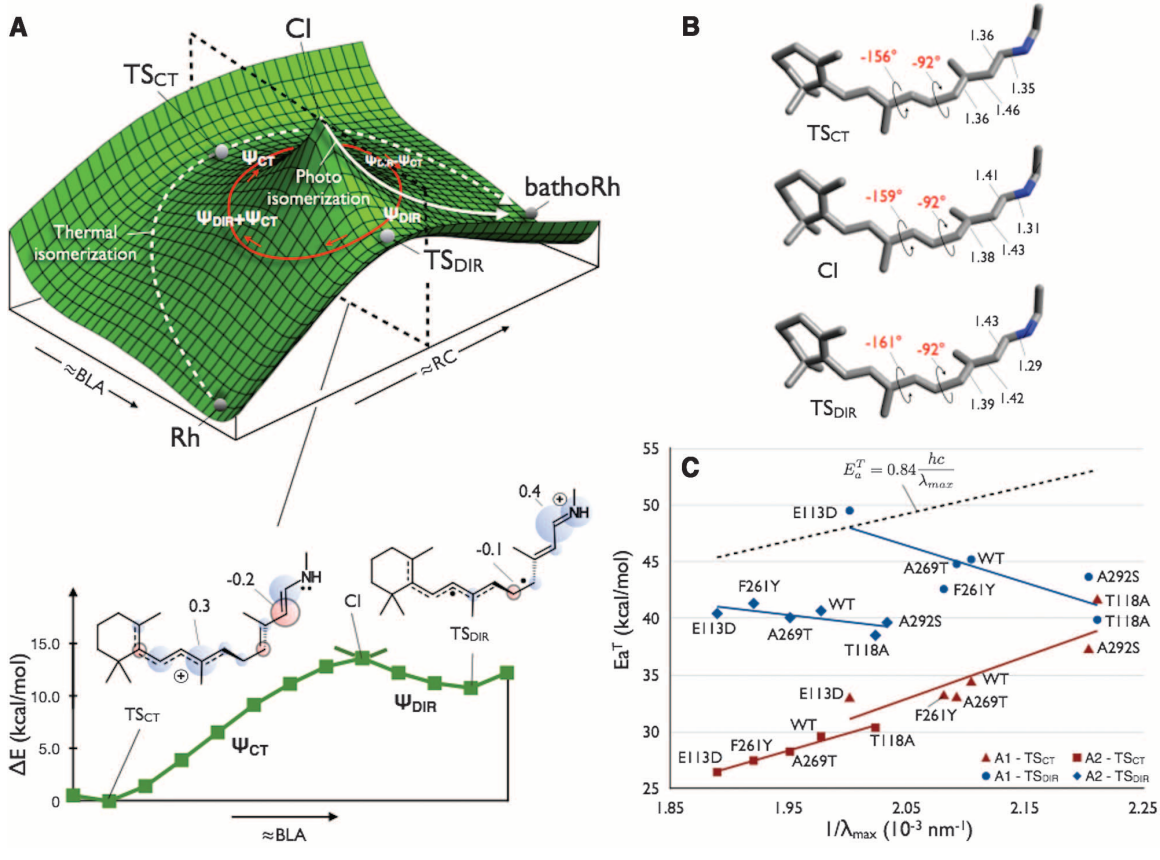

Fig. 2. (**A**) Schematic overview of the S_0 potential energy surface driving the thermal isomerization of bovine Rh, represented by the isomerization coordinate RC. A second coordinate BLA (corresponding to the elongation of double bonds coupled with a shortening of single bonds and connecting TS_{CT}, CI, and TS_{DIR}) is shown in addition to RC. The loop represents the electronic wavefunction changes associated with the presence of a CI. The CASPT2//CASSCF/6-31G*/AMBER relative energy change computed along the BLA coordinate (bottom) shows that TS_{CT} is the lowest energy point separating the reactant from the product energy minima. The S_0 Mulliken charge distributions of TS_{CT} and TS_{DIR} are represented with a bubble diagram, and the bond-line formulas represent the associated dominant electronic configuration (e.g., ψ_{DIR} for TS_{DIR}, S_0 Rh, and bathoRh; and ψ_{CT} for TS_{CT} and S_1 Rh). A region of the S_0 potential energy surface with ψ_{CT} character was also discussed in ref. (*31*). (**B**) CASSCF/6-31G*/AMBER geometrical parameters (in angstroms and degrees) of the TSs driving the thermal isomerization of bovine Rh compared with the corresponding CI values (the CI structure here is the one found along the BLA scan at the bottom of Fig. 2A). (**C**) CASPT2//CASSCF/6-31G*/AMBER-computed E_a^T values versus $1/\lambda_{max}$ for bovine Rh (WT), bovine opsin with the A2 chromophore (WT-A2), and their mutants. The lines indicates linear regression. The dashed line corresponds to the observed ratio described in Luo *et al.* (*16*).

the reported TS_{DIR} and TS_{CT} structures located along the BLA coordinate on opposite sides of the CI appear to be a manifestation of the geometric-phase theorem.

The key to understanding the origin of the thermal noise in rod photoreceptors is the existence of two electronically different TSs, with the lower displaying the same charge-transfer character as the Rh excited state. This is a consequence of the properties of the chromophore electronic wavefunction in the region of the CI (*27*, *28*, *30*). Therefore, the Barlow correlation represents a manifestation of the existence of a CI in Rh and complements the evidence provided by spectroscopic studies (*3*–*5*, *9*). Without this CI, the thermal isomerization would be controlled by the TS_{DIR} barrier and, therefore, high visual sensitivity would be achieved at the red edge of the visible spectrum rather than the blue. Further evidence supporting this theory could be provided by the observation of an "anti-Barlow" correlation (i.e., a decrease of $-\log k$ as a function of $1/\lambda_{max}$) for mutants or pigments containing PSB11 but absorbing radiations shorter than 470 nm.

References and Notes

1. A. Terakita, *Genome Biol.* **6**, 213 (2005).
2. G. Wald, *Nature* **219**, 800 (1968).
3. R. W. Schoenlein, L. A. Peteanu, R. A. Mathies, C. V. Shank, *Science* **254**, 412 (1991).
4. H. Kandori, Y. Shichida, T. Yoshizawa, *Biochemistry (Mosc.)* **66**, 1197 (2001).
5. P. Kukura, D. W. McCamant, S. Yoon, D. B. Wandschneider, R. A. Mathies, *Science* **310**, 1006 (2005).
6. Q. Wang, R. W. Schoenlein, L. A. Peteanu, R. A. Mathies, C. V. Shank, *Science* **266**, 422 (1994).
7. T. Andruniów, N. Ferré, M. Olivucci, *Proc. Natl. Acad. Sci. U.S.A.* **101**, 17908 (2004).
8. L. M. Frutos, T. Andruniów, F. Santoro, N. Ferré, M. Olivucci, *Proc. Natl. Acad. Sci. U.S.A.* **104**, 7764 (2007).
9. D. Polli *et al.*, *Nature* **467**, 440 (2010).
10. M. G. Khrenova, A. V. Bochenkova, A. V. Nemukhin, *Proteins* **78**, 614 (2010).
11. D. A. Baylor, G. Matthews, K. W. Yau, *J. Physiol.* **309**, 591 (1980).
12. G. A. Schick, T. M. Cooper, R. A. Holloway, L. P. Murray, R. R. Birge, *Biochemistry* **26**, 2556 (1987).
13. A. P. Sampath, D. A. Baylor, *Biophys. J.* **83**, 184 (2002).
14. J. Liu *et al.*, *J. Am. Chem. Soc.* **131**, 8750 (2009).
15. P. Ala-Laurila, K. Donner, A. Koskelainen, *Biophys. J.* **86**, 3653 (2004).
16. D. G. Luo, W. W. Yue, P. Ala-Laurila, K. W. Yau, *Science* **332**, 1307 (2011).
17. R. B. Barlow, R. R. Birge, E. Kaplan, J. R. Tallent, *Nature* **366**, 64 (1993).
18. J. Liu *et al.*, *J. Biol. Chem.* **286**, 27622 (2011).
19. V. A. Lórenz-Fonfría, Y. Furutani, T. Ota, K. Ido, H. Kandori, *J. Am. Chem. Soc.* **132**, 5693 (2010).
20. I. Bókkon, R. L. Vimal, *J. Photochem. Photobiol. B* **96**, 255 (2009).
21. V. R. Kaila, R. Send, D. Sundholm, *J. Phys. Chem. B* **116**, 2249 (2012).
22. H. B. Barlow, *Nature* **179**, 255 (1957).
23. P. Ala-Laurila, J. Pahlberg, A. Koskelainen, K. Donner, *Vision Res.* **44**, 2153 (2004).
24. L. De Vico, M. Olivucci, R. Lindh, *J. Chem. Theory Comput.* **1**, 1029 (2005).
25. Materials and methods are available as supplementary materials on *Science* Online.
26. S. J. Milder, *Biophys. J.* **60**, 440 (1991).
27. G. Herzberg, H. C. Longuet-Higgins, *Discuss. Faraday Soc.* **35**, 77 (1963).
28. G. J. Atchity, S. S. Xantheas, K. Ruedenberg, *J. Chem. Phys.* **95**, 1862 (1991).
29. P. B. Coto, A. Sinicropi, L. De Vico, N. Ferre, M. Olivucci, *Mol. Phys.* **104**, 983 (2006).
30. S. Zilberg, Y. Haas, *Photochem. Photobiol. Sci.* **2**, 1256 (2003).
31. A. Warshel, *Proc. Natl. Acad. Sci. U.S.A.* **75**, 2558 (1978).

Acknowledgments: We are grateful to M. A. Robb for a critical reading of the manuscript. This work was supported by the Bowling Green State University. M.O. is grateful to the Center for Photochemical Sciences and the School of Arts and Sciences of Bowling Green State University for startup funds. We are grateful to the Ohio Supercomputer Center for granted computer time.

Supplementary Materials

www.sciencemag.org/cgi/content/full/337/6099/1225/DC1
Materials and Methods
Figs. S1 to S11
Tables S1 to S6
References (*32*–*92*)

13 February 2012; accepted 2 July 2012
10.1126/science.1220461

Ecological Populations of Bacteria Act as Socially Cohesive Units of Antibiotic Production and Resistance

Otto X. Cordero,[1]* Hans Wildschutte,[1]* Benjamin Kirkup,[1]* Sarah Proehl,[1] Lynn Ngo,[1] Fatima Hussain,[1] Frederique Le Roux,[2] Tracy Mincer,[3] Martin F. Polz[1]†

In animals and plants, social structure can reduce conflict within populations and bias aggression toward competing populations; however, for bacteria in the wild it remains unknown whether such population-level organization exists. Here, we show that environmental bacteria are organized into socially cohesive units in which antagonism occurs between rather than within ecologically defined populations. By screening approximately 35,000 possible mutual interactions among Vibrionaceae isolates from the ocean, we show that genotypic clusters known to have cohesive habitat association also act as units in terms of antibiotic production and resistance. Genetic analyses show that within populations, broad-range antibiotics are produced by few genotypes, whereas all others are resistant, suggesting cooperation between conspecifics. Natural antibiotics may thus mediate competition between populations rather than solely increase the success of individuals.

The ratio of intra- versus interspecific competition is a key element regulating populations and determining their success within diverse communities. It is especially important in structured animal and plant populations, in which closely related individuals live in patches and encounter each other often (*1*). In these cases, modulation of intraspecific antagonism or cooperation can mitigate the detrimental effects of niche overlap. However, for bacteria in the wild it has been postulated that populations merely represent loose assemblages of individuals driven by ecological opportunity (*2*, *3*). The reasons given include high dispersal rates and rapid horizontal gene transfer (HGT), which can both rapidly erode population structure by mixing unrelated individuals and introducing novel, potentially advantageous genes to their genomes. This may initiate a dynamic process of rapid but locally and/or temporarily limited expansion of individuals (clones). A classical example of such interactions is interference competition via colicin-type bacteriocins (*4*, *5*), which are almost always encoded by plasmids and are able to kill closely related competitors in a highly specific manner. In these cases, population dynamics are primarily driven by the cyclic invasion of antibiotic production and resistance genes. Similarly, a recent high-throughput screen of mutual interactions among soil isolates indicated changing types of interactions occur over relatively short evolutionary distances. This was interpreted as short-lived dynamics of gene gain and loss, in which antibiotic production selects resistance, which subsequently promotes loss of production and reversion to sensitivity (*6*). In contrast to this gene-centric view of bacterial population dynamics, recent fine-scale environmental mapping of bacterial diversity has suggested that population structure may exist beyond individual clones. Such ecologically defined populations consist of phylogenetic clusters of closely related but nonclonal individuals, which share common ecological associations (*7*, *8*). However, it remains unknown whether individuals within such populations interact sufficiently strongly to allow for

[1]Department of Civil and Environmental Engineering, Massachusetts Institute of Technology, Cambridge, MA 02139, USA. [2]Laboratoire de Génétique et Pathologie BP 133, Insititut Français de Recherche pour l'Exploitation de la Mer, 17390 La Tremblade, France. [3]Department of Marine Chemistry and Geochemistry, Woods Hole Oceanographic Institution, Woods Hole, MA 02543, USA.

*These authors contributed equally to this work.
†To whom correspondence should be addressed. E-mail: mpolz@mit.edu